AIAA JOURNAL
Vol. 55, No. 5, May 2017

Ultrasonic-Attenuation-Based Technique for Ice Characterization Pertinent to Aircraft Icing Phenomena

Yang Liu,* Leonard J. Bond,† and Hui Hu‡
Iowa State University, Ames, Iowa 50010

DOI: 10.2514/1.J055500

A novel approach, which is capable of characterizing different types of ice accretion, was developed by leveraging the significant discrepancies in attenuation characteristics of ultrasonic waves traveling in different ice types (i.e., rime or glaze). While the theories of acoustic attenuation in pulse-echo configuration for a multilayer structure were formulated, a feasibility study was also performed to demonstrate the ultrasonic-attenuation-based technique to characterize two different types of ice samples representative of typical rime and glaze ice accretion seen over airframe surfaces. Significant differences were found in the ultrasonic attenuation characteristics between the two compared ice samples over the frequency range of 5–15 MHz. The attenuation coefficients of the rime-like ice sample were found to be much greater than those of the glaze-like ice sample at any given ultrasonic frequencies. While the values of ultrasonic attenuation coefficients would increase with ultrasonic frequency for both the ice samples, the attenuation coefficients of the rime-like ice were found to have a much greater increasing slope (i.e., $d\alpha/df$) and wider scattering range than those of the glaze-like ice. Such information could be used to develop ice-type-specific de-icing systems to reduce de-icing operational costs for aircraft operation in cold climate.

Nomenclature

A_0	=	amplitude of an ultrasonic wave at the transducer front
B	=	Fourier transform of actual ultrasonic pulse
C	=	factor of beam spread
c	=	phase velocity of ultrasonic wave in propagation medium
d	=	thickness of top layer in ultrasonic measurement, cm
F_0	=	Fourier transform of ultrasonic pulse
h	=	thickness of ice layer in ultrasonic measurement, cm
k	=	wave propagation constant
R	=	reflection coefficient at an interface
T	=	transmission coefficient at an interface
U	=	acoustic velocity in ice layer
u	=	voltage of ultrasonic pulse
Z	=	acoustic impedance of material
z	=	equivalent path length
α	=	attenuation coefficient of ultrasonic wave
β	=	system efficiency factor
Δt	=	time interval between the echoes from two interfaces
ω	=	angular frequency of ultrasonic wave

I. Introduction

AIRCRAFT icing has been considered as one of the most serious hazards to impact flight safety [1]. Ice accretion can destroy the smooth airflow over lift and control surfaces, which decreases the ability of aircraft to generate lift [2]. Additionally, the uncontrolled shedding of ice that has built up on aircraft surfaces may severely damage aircraft components [3]. From an economic perspective, ice accretion can increase the costs of flight operations due to the use of anti/de-icing equipment and fluids. Moreover, the time spent in performing de-icing procedure can cause flight delays or even cancelations, which can then significantly impact airline performance and, hence, total operation costs [4]. The morphology of ice accretion on aircraft surface can be either rime or glaze, depending on weather conditions [5]. Rime ice usually forms at low air temperatures (typically below −10°C) when aircraft fly through clouds with low liquid water content (LWC) and small water droplets. Such rime ice appears to be white and opaque, and it is formed containing many microbubbles and cracks [6]. If the air temperature is relatively high (i.e., just below the freezing point), glaze ice tends to form, especially when an aircraft encounters cloud with a higher LWC and larger super-cooled droplets. In the case of glaze ice accretion, the impinged droplets will deform and run back over the aircraft surfaces as liquid before freezing downstream, which results in smooth, clear, and dense ice shapes [6]. Because of the different physical mechanisms occurred in the two icing processes, rime ice generally conforms to the shape of aircraft surfaces, and it therefore has a smaller effect on aircraft performance, whereas glaze ice forms and covers more surfaces and has a more severe effect on the aircraft flight performance.

To reduce the potential harmful effects of aircraft icing, a number of anti/de-icing systems have been developed, which can be considered in three groups, including freezing-point depressants, thermal melting, and surface deformation [7]. With these anti/de-icing approaches, the amount and the rate of ice removal are mainly determined by the volume of de-icing fluid or electrical power applied. For rime ice accretion, because of the porous nature of the structures in ice layers and typically smaller area on the aircraft surfaces on which it forms, it is relatively easier to remove. In comparison, glaze ice is much denser and typically has a higher adhesion to aircraft surfaces and extends farther downstream on a wing surface over a larger area. Therefore, more de-icing fluid or power is required to remove glaze ice accretion [7]. In looking at performance optimization, most of the current de-icing systems were, however, developed without considering the characteristics of the accreted ice. De-icing systems are usually operated using the same procedures and strategies, regardless of the ice type. As a result, a lot of potentially unnecessary de-icing actions are performed during flight operations to ensure effective removal of ice on aircraft surfaces [8,9]. In looking to improve flight operational performance in cold weather, methods and techniques for ice detection and characterization are highly desirable that can potentially improve and optimize de-icing.

To address this need, many ice detection and monitoring techniques have been investigated, which use either direct or indirect measurement approaches. Indirect measurement approaches usually detect icing events based on monitoring flight performance metrics, such as a lift decrease or drag increase, or from measurements of weather conditions, such as air humidity and temperature [4,10].

Received 31 July 2016; revision received 12 October 2016; accepted for publication 19 November 2016; published online 30 January 2017.

*Postdoctoral Associate, Department of Aerospace Engineering.
†Professor, Department of Aerospace Engineering.
‡Martin C. Jischke Professor, Department of Aerospace Engineering; huhui@iastate.edu. Associate Fellow AIAA (Corresponding Author).

As ice forms on aircraft surfaces, the flight performance can be affected very quickly. Therefore, for safety reasons, direct methods for ice detection are generally preferable. Most of the direct measurement approaches provide icing warnings with data from measuring aircraft surface properties with changes in mass, reflective index, electrical/thermal conductivity, dielectric coefficient, or inductance, in which extensive physical principles were used (i.e., vibration [11], electrooptical [12], fiber-optical [13], radio frequency [14], micromechanical sensor [15], and inductive devices [16]). For many of these techniques, however, only laboratory implementations have been achieved due to the constraints in real applications. For example, the diaphragm sensors and the electrooptical sensors are required to be flush-mounted on the exterior surface of an aircraft, which is not desirable because they may affect the aircraft aerodynamic performance. The fiber-optic sensor requires a light transmission window for signal sending/receiving, which could also be a big challenge for aircraft implementations [9].

Ultrasonic techniques have been widely studied and applied for aircraft icing researches [8]. As reported by Hansman and Kirby [17], an ultrasonic pulse-echo technique was developed to provide real-time thickness measurements of rime and glaze ice accretion. The water/ice layers were characterized using ultrasonic echoes where signals were generated at interfaces. The interface reflections were displayed on an oscilloscope for qualitative analysis of the rime and glaze accretion process. Ultrasonic guided-wave technologies have also been developed in recent years for ice detection and classification based on the dispersion characteristics of the phase and group velocity curves for waves in the multilayer system [8,18,19]. Although great details of the modeling concepts and numerical calculations on the wave propagation characteristics for different types of ice were presented in those studies, only very limited experimental data, without classification of different ice types, were given to validate the model predictions [8].

In terms of implementations on aircraft, various ultrasonic transducers and systems have been fabricated to provide in situ ice detection. One example of a recent implement was that provided by Liu et al. [20], who developed two types of flexible ultrasonic sensors that were used to monitor in situ structural thickness and ice buildup. These transducers were easily attached on the inside of the curved airfoil surfaces on aircraft.

In the present study, a new ultrasonic-attenuation-based approach, which is capable of quantitatively characterizing the types (i.e., rime or glaze) and thickness of ice accretion pertinent to aircraft icing phenomena, is introduced to further extend the capability of ice detection and characterization with ultrasonic techniques. The new method is developed by leveraging the discrepancies in attenuation characteristics of the ultrasonic waves traveling in test samples of different ice types as reported in previously published literatures [21–24]. In the text that follows, the fundamental basis and theories for ultrasonic attenuation in pulse-echo mode are introduced briefly at first. Then, two different types of ice samples representative of rime and glaze ice accretion typically seen over aircraft surfaces are characterized based on attenuation of ultrasonic waves in a pulse-echo configuration. A feasibility study is also performed to demonstrate the implementation of the ultrasonic-attenuation-based technique by analyzing the measured ultrasonic attenuation characteristics of the two ice samples along with quantitative comparison of the measurement results with the data reported in previously published literature.

II. Theories for Ultrasonic Attenuation in Pulse-Echo Mode

In a typical ultrasonic pulse-echo measurement, the ultrasonic pulse is first emitted into the object being investigated using a transducer. If the object is composed of multiple layers with different acoustic impedances, the ultrasonic waves will be partially transmitted/reflected at each of the layer interfaces. The reflected waves (i.e., echoes) will be detected by the same transducer and measured as a voltage–time signal. Such ultrasonic pulse-echo measurements are commonly used in ultrasonic thickness gages, in which the material thickness is measured by determining the time interval between the various waves reflected from the interfaces [25].

When ultrasonic wave travels through a medium, its intensity diminishes with distance. In a nonattenuating ideal material, the wave amplitude is only reduced by the beam spread. In real materials, however, the wave is also reduced in amplitude by scattering and absorption. The combined effects of scattering and absorption cause what is known as attenuation [26]. Ultrasonic attenuation is defined as the decay of wave amplitude as it propagates through a material. In the present study, ice samples with different internal morphologies were characterized using an ultrasonic pulse-echo method, where the ultrasonic attenuation is expected to vary due to differences in the ice crystal structure and the porosity, which cause scattering.

A schematic of the propagation paths of ultrasonic waves in pulse-echo in a multilayer object is shown in Fig. 1. In this multilayer model, the top and bottom layers are made of the same material, and the sample layer being measured, which in this case is the ice, is sandwiched between these plates. As the ultrasonic waves travel through the top layer, a fraction of the energy is reflected at the first interface (i.e., ice–top interface), whereas the remainder is transmitted into the ice and then partially reflected at the second interface (i.e., ice–bottom interface).

The ultrasonic waves traveling in the multilayer model can be described by the basic equation [Eq. (1)] for a progressive wave [27]:

$$A = A_0 e^{-\alpha x} \cos(kx - \omega t) \tag{1}$$

where A is the amplitude of the ultrasonic wave along the X coordinate; A_0 is the amplitude of the ultrasonic wave at the origin ($x = 0$); α is the attenuation coefficient; k is the propagation constant ($k = 2\pi/\lambda = \omega/c$); ω is the angular frequency ($\omega = 2\pi f$); and c is the phase velocity in propagation medium.

For a conventional ultrasonic transducer, the ultrasonic pulse is a superposition of harmonic waves with many different frequencies, and it can be expressed as shown in Eq. (2) [27]:

$$u(x,t) = \frac{1}{2\pi}\int_{-\infty}^{\infty} F_0(\omega) e^{-\alpha x} \cos(kx - \omega t)\mathrm{d}\omega \tag{2}$$

where $F_0(\omega)$ can be given by the Fourier transform of $u(0,t)$.

The signal that is measured for the reflected waves is a combination of the pressure signals that are, in effect, convolved,

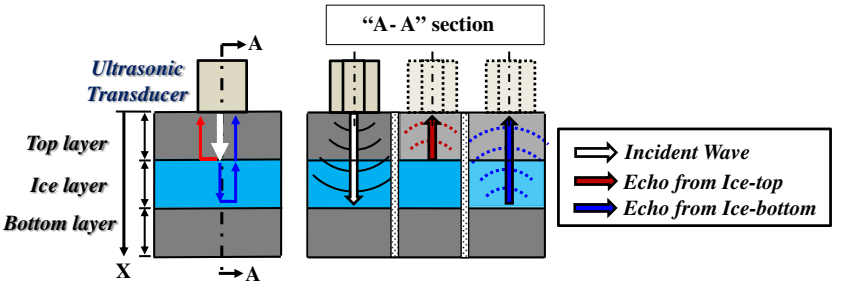

Fig. 1 Schematic of the ultrasonic pulse-echo paths in a multilayer object.

with the transducer and electronics characteristics, the reflection and transmission at interfaces, as well as the beam spread. Therefore, to describe the measured ultrasonic pulse-echo waves, additional terms need to be added, and these are given in Eq. (3):

$$u_n = \frac{1}{2\pi}\int_{-\infty}^{\infty}[\beta(\omega)\cdot R\cdot T\cdot C_n(\omega)\cdot F_0(\omega)e^{-\alpha x}]e^{-j\omega t}\,\mathrm{d}\omega \quad (3)$$

where $\beta(\omega)$ is the system efficiency factor, R and T are the reflection and transmission coefficients at the interfaces, and $C_n(\omega)$ describes the effects of beam spread.

The ultrasonic attenuation in the ice layer was derived by comparing the amplitude spectra of the primary echoes (i.e., the first echoes in time sequence) that are reflected from the ice–top and bottom interfaces. The Fourier transform of u_n can be expressed in the form given as Eq. (4):

$$B(u_n) = B(\omega) = B(f) = \beta(\omega)\cdot R\cdot T\cdot C_n(\omega)\cdot F_0(\omega)e^{-\alpha x} \quad (4)$$

If the thickness of the top layer is d, the amplitude spectrum of the primary echo from the ice–top interface can be written as

$$B_0(f) = \beta(f)T_{01}R_{12}T_{10}C(2d,f)F_0(f)e^{-2\alpha_0 d} \quad (5)$$

where T_{01} and T_{10} are the transmission coefficients when the ultrasonic waves travel forward and backward through the ice–top interface; R_{12} is the reflection coefficient at the ice–top interface; $C(2d,f)$ is the beam diffraction correction term in the top layer; and α_0 is the ultrasonic attenuation coefficient in the top layer.

To formulate the amplitude spectrum of the primary echo from the ice–bottom interface, the diffraction term was first calculated using an equivalent path length z, which is equal to the summation of the actual path length in the top layer and the equivalent path length of the ice layer in the top layer, which is given as Eq. (6):

$$2z = 2d + \frac{U_{\text{ice}}}{U_1}2h \quad (6)$$

where U_{ice} and U_1 are the sound velocities in the ice layer and top layer, and h is the thickness of the ice layer. Therefore, the amplitude of the primary echo from the ice–bottom interface can be derived, and this is shown as Eq. (7):

$$B_1(f) = \beta(f)T_{01}T_{12}R_{23}T_{21}T_{10}C(2z,f)F_0(f)e^{-2\alpha_0 d}e^{-2\alpha_1 h} \quad (7)$$

where T_{12} and T_{21} are the transmission coefficients when the ultrasonic waves travel forward and backward through the ice–bottom interface, and R_{23} is the reflection coefficient at the ice–bottom interface. $C(2z,f)$ is the equivalent beam diffraction for the primary echo from the ice–bottom interface; $\alpha_1(f)$ is the ultrasonic attenuation coefficient in the ice layer. The reflection coefficients at the ice–top and ice–bottom interfaces are given as Eqs. (8) and (9):

$$R_1 = R_{12} = R_{21} = \left|\frac{Z_{\text{ice}} - Z_1}{Z_1 + Z_{\text{ice}}}\right| \quad (8)$$

$$R_2 = R_{23} = R_{32} = \left|\frac{Z_2 - Z_{\text{ice}}}{Z_{\text{ice}} + Z_2}\right| \quad (9)$$

where Z_1 and Z_2 are the acoustic impedances of the top and bottom layers, and Z_{ice} is the acoustic impedance of the ice layer. The relationships between the transmission coefficient and reflection coefficient at the two interfaces are given as Eqs. (10) and (11):

$$T_{01}\cdot T_{10} = 1 - R_0^2 \quad (10)$$

$$T_{12}\cdot T_{21} = 1 - R_1^2 \quad (11)$$

The beam diffraction correction term has been derived and evaluated in many studies. Here, an exact expression for the Lommel diffraction correction integral derived by Rogers and Van Buren [28] was applied, and this is in the form shown as Eq. (12).

$$C = 1 - e^{-(2\pi/s)i}[J_0(2\pi/s) + iJ_1(2\pi/s)] \quad (12)$$

where $s = 2\pi z/ka^2$; $k = \omega/V$; $\omega = 2\pi f$; J_0 and J_1 are Bessel functions of the first kind; and a is the radius of the circular piston source. The magnitude of the diffraction correction is more usually given in a simpler form as shown in Eq. (13):

$$|C| = \left\{\begin{array}{l}[\cos(2\pi/s) - J_0(2\pi/s)]^2\\ +[\sin(2\pi/s) - J_1(2\pi/s)]^2\end{array}\right\}^{1/2} \quad (13)$$

The correction terms are used in the amplitude spectrum equations [Eqs. (5) and (7)]. By comparing the two frequency-dependent amplitude spectra [Eq. (14)], the ultrasonic attenuation in the sample layer, which in this case is ice, can be derived and is given in Eq. (15):

$$\frac{B_0(f)}{B_1(f)} = \frac{R_1}{(1-R_1^2)R_2}\frac{C(2d,f)}{C(2z,f)}e^{2\alpha_1 h} \quad (14)$$

$$\alpha_1(f) = \frac{1}{2h}\left[\ell_n\frac{B_0(f)}{B_1(f)} - \ell_n\frac{C(2d,f)}{C(2z,f)} - \ell_n\frac{R_1}{(1-R_1^2)R_2}\right] \quad (15)$$

In the present study, the time-domain responses of the echoes from the ice–top and ice–bottom interfaces were measured using an ultrasonic pulse-echo technique. The amplitude spectra of the echo waves were calculated by using a fast Fourier transform (FFT). Because the correction terms have been quantitatively evaluated, the frequency-dependent ultrasonic attenuation coefficient can be calculated.

III. Experimental Evidence

A. Experimental Setup for the Attenuation Measurements

A schematic of the experimental setup for the attenuation measurements with an ultrasonic pulse-echo method is shown in Fig. 2. In the present study, two well-polished aluminum plates were used as the top and bottom layers, and the measured layer was deposited in between the two plates. The top and bottom plates were fixed so as to be parallel and placed within a low-temperature-resistant plastic tank, in which various materials can be deposited (e.g., water, ice). The ultrasonic transducer, with element diameter of 3.175 mm (0.125 in.) and nominal center frequency of 10 MHz, was attached to the top plate and connected to the pulser/receiver as shown in the figure. The pulser/receiver was a modified commercial ultrasonic inspection unit (Omniscan iX), which has a sampling frequency of 100 MHz. Although the pulser/receiver was used to generate and receive pulse-echo signals, a host computer was used to control the measurements and to collect and process the pulse-echo signals.

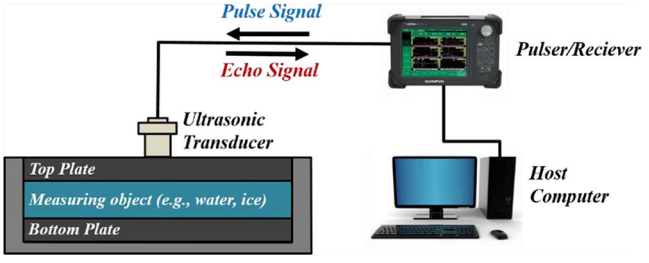

Fig. 2 Experimental setup for the attenuation measurement with ultrasonic pulse-echo method.

The integration of the ultrasonic transducer, pulser/receiver, and host computer forms a typical ultrasonic pulse-echo system. The Omniscan iX unit is designed to operate with a phased array and was modified so as to be capable of generating, amplifying, and sending voltage pulses to multiple discrete ultrasonic transducers. With the high-voltage excitation, the transducer will emit ultrasonic pulses into the test sample. As the pulses arrive at interfaces, they are partially reflected, and signals are received by the transducer. The echo signal is received, amplified, and digitized in the Omniscan iX unit. Semicustom software is used to control the system functions, signal generation, data collection, and processing in the host computer.

B. Validation of the Ultrasonic Attenuation Model

To validate the theoretical model for calculation of the ultrasonic attenuation in the multilayer object, data for determining ultrasonic attenuation in water were first collected, processed, and examined. The plastic tank was filled with distilled water at room temperature. The methodology developed in this study, for determining the ultrasonic attenuation, was then applied to the sequence of echo signals.

The data for ultrasonic attenuation in water (at room temperature), as a function of frequency, are shown as Fig. 3. The proposed methodology, as well as software implementation, was validated by comparing the results from the present experiments with the data for ultrasonic attenuation in water (at room temperature) previously reported by Krautkrämer and Krautkrämer [29]. It is seen that there is good agreement with attenuation based on fundamental physical constants.

The measurement accuracy in the present work was mainly limited by the digitizing resolution in the ultrasonic pulse-echo system. Based on the uncertainty analysis, the attenuation measurement accuracy was estimated to be ± 0.003 Np/cm, and there was a correlation coefficient of 98% between the data sets.

C. Ultrasonic Attenuation in Ice Samples

1. *Ice Sample Preparation*

The two forms of ice investigated in the present study are rime and glaze ice, which are typically seen for in-flight ice accretions over aircraft surfaces. While the forms of rime and glaze ice were only described qualitatively in most of previous studies [2,6,30], a process was developed in the present study to prepare rime-like and glaze-like ice test samples to obtain quantitative measurement data of the ice samples. A series of water distillation and forced freezing procedures were developed to prepare samples that are, at least in qualitative terms, similar to those previously reported [31] for rime and glaze ice.

To prepare the rime-like ice sample, the plastic tank with the fixed aluminum plates was placed in a refrigerator with the temperature set

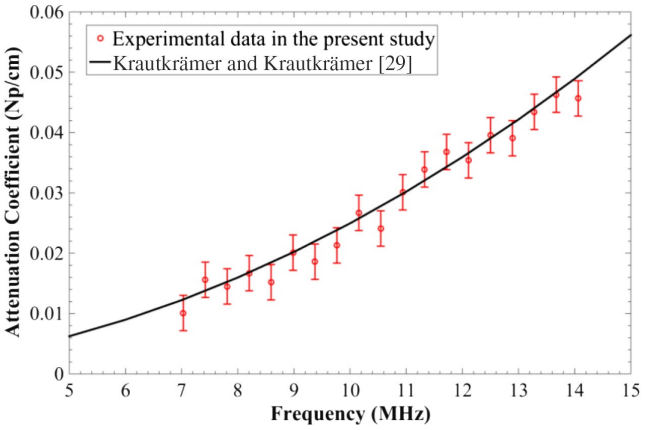

Fig. 3 Comparison of ultrasonic attenuation in water from the present experiments and the previously reported results by Krautkrämer and Krautkrämer [29].

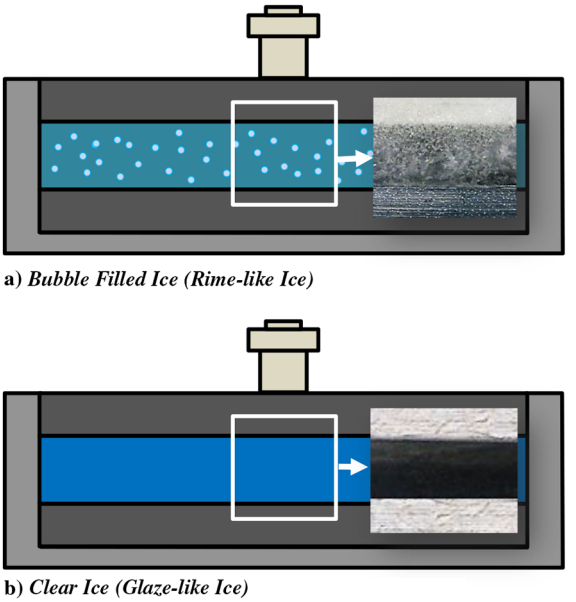

a) ***Bubble Filled Ice (Rime-like Ice)***

b) ***Clear Ice (Glaze-like Ice)***

Fig. 4 Laboratory prepared ice samples representing a) rime, and b) glaze ice structures.

below −10°C, whereas water was chilled to near 0°C. When the aluminum plates were chilled to below −10°C, the near zero-degree water was sprayed onto the bottom plate. It was found that, as the droplets impacted on the aluminum surface, they froze immediately. Small ice particles formed and built up between the plates. An ice layer containing many air bubbles and ice grains was formed as shown in Fig. 4a. The ice sample appeared to be very opaque and white with void randomly distributed, which is similar to the rime ice samples used in previous studies [30].

To prepare a glaze-like ice sample, water was double-boiled to eliminate dissolved air. The sample was permitted to cool between boiling, and an interval of 30 min was left between the boiling operations. The double-boiled water was then slowly added into the plastic tank to fill the gap between the top and bottom aluminum plates. The tank was then placed in the refrigerator, with temperature set at −5°C. An ice layer gradually formed with no observable bubbles or cracks trapped inside, as shown in Fig. 4b. The ice sample processed in such a manner appeared to be very dense and clean, which is similar to the glaze ice samples observed in both ground and in-flight aircraft icing tests [5,17,31].

2. *Acoustic Velocity in Ice samples*

To enable calculation of the wave reflection coefficient [Eqs. (8) and (9)] at interfaces, it is necessary to first evaluate the acoustic velocity and impedance in the ice samples. The acoustic velocity was determined by measuring the time-of-flight and propagation path and the relationship is shown as Eq. (16) [25]:

$$U = \frac{2h}{\Delta t} \tag{16}$$

where U is the acoustic velocity in the ice layer, h is the thickness of the ice layer, and Δt is the time interval between the echoes reflected from the ice–top and ice–bottom interfaces. In this study, the thickness of the ice layer (i.e., the gap between the aluminum plates) was measured to be 6.00 ± 0.02 mm using a digital caliper.

Examples of the time-domain responses of the ultrasonic pulse-echo signals in the rime-like and glaze-like ice samples are shown in Fig. 5. In both of the ice samples, two echo sequences can be observed, with one being from the ice–top interface and the other from the ice–bottom interface.

To find the time intervals between the pulses in the echo sequences, an autocorrelation algorithm was applied to the digitized waveforms [32]. The correlation process gave the transit time interval by

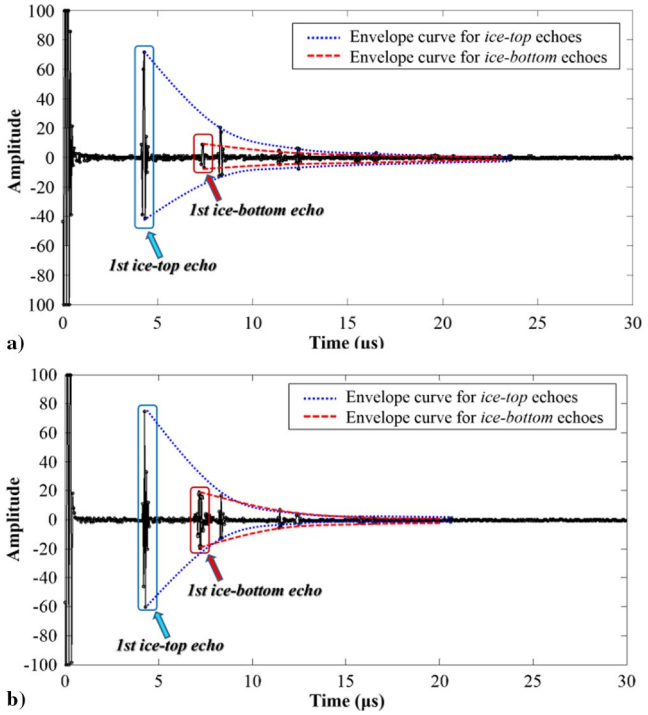

Fig. 5 Ultrasonic pulse-echo signals in the a) rime-like, and b) glaze-like ice samples.

measuring the time delay between the corresponding peaks in the autocorrelation function. For example, the time delay between the ice–top and ice–bottom echoes for the rime-like ice sample was 3.05 ± 0.05 μs, whereas the time delay for the glaze-like ice sample was 3.15 ± 0.05 μs. Thus, the acoustic velocity in the two ice samples can be calculated using Eq. (16), and these velocities are 3.93 ± 0.08 and 3.80 ± 0.08 mm/μs for the rime-like and glaze-like ice samples, respectively.

The velocities measured using the preceding method were compared with previously reported values [31,33–35], and selected data are given in Table 1. It can be seen that the acoustic velocity only exhibits a modest sensitivity to ice types [31]. The data values for velocity from the present study are in agreement with the values given by Hansman and Kirby [31]. The acoustic velocity in the rime-like ice sample is slightly faster than that in the glaze-like ice sample. In addition to any differences due to composition (ice and bubbles), it has been previously found that sound speed in ice is temperature-dependent, with a faster velocity being seen at lower temperatures [33].

The densities for the samples were measured using $\rho = \mathrm{m/V}$, where ρ is the density, m is the mass of the ice sample that can be measured using the OHAUS Scout® Pro Balance with an accuracy of ± 0.01 g, and V is the volume of the ice sample (i.e., the gap volume between the top and bottom plates). The densities for the rime-like and glaze-like ice samples are measured to be 0.88 ± 0.02 and 0.90 ± 0.02 g/cm^3, respectively. It has been previously demonstrated by Vargas et al. [36] that the ice density does not change significantly when the morphology of the ice changes. The only changes are when there are bubbles present. The ice densities measured in the present study are consistent with those for rime and glaze ice reported by Vargas et al. [36] as shown in Table 2. These density and velocity data were then used to calculate the acoustic impedance (i.e., $Z = \rho c$) in the ice samples.

Table 1 Acoustic velocities in ice

Ice type	Acoustic velocity in ice, mm/μs	Data source
General ice	3.98	Filipczynski et al. [35]
South Pole ice	3.85 (at zero depth)	Abbasi et al. [34]
Bubble-free ice	3.87 ($T = -10$°C)	Vogt et al. [33]
Bubble-free ice	3.85 ($T = -5$°C)	Vogt et al. [33]
Rime ice	3.93	Hansman and Kirby [31]
Rime ice	3.95 ($T = -10$°C)	Present study
Glaze ice	3.78	Hansman and Kirby [31]
Glaze ice	3.80 ($T = -5$°C)	Present study

3. *Ultrasonic Attenuation in the Ice Samples*

The reflection and transmission terms were calculated using Eqs. (8–11), and the diffraction correction was estimated using Rogers and Van Buren's theory [28]. The frequency-dependent ultrasonic attenuation coefficients for the ice samples were then determined using the amplitude spectra, obtained from the digitized ultrasonic pulse-echo signals. A fast Fourier transform (FFT) was applied to gated segments (with a length of 1.5 μs) of the time-domain response that correspond to the echoes reflected from the ice–top and ice–bottom interfaces.

The amplitude spectra of the reflected signals from the ice–top and ice–bottom interfaces for the rime-like ice sample are shown in Fig. 6a. It is seen that, for each signal, it has a center frequency close to 10 MHz, which corresponds to the transducer nominal frequency. The amplitude diminishes to near zero at frequencies lower than about 3 MHz and higher than about 18 MHz. A band-pass filter with −6 dB bandwidth was applied to minimize possible effects of processing low-amplitude signals and noise on the attenuation coefficient. Because the beam diffraction correction and wave reflection coefficient have been quantitatively evaluated [Eqs. (8–13)], by comparing the two frequency-dependent amplitude spectra as shown in Eq. (14), the responses are then deconvolved to obtain a frequency-dependent attenuation coefficient in the frequency range of 5.5–14.0 MHz using Eq. (15) for the rime-like ice sample as shown in Fig. 7.

A similar process was applied to the data shown in Fig. 5b for the glaze-like ice sample. The spectra for the two signals are shown in Fig. 6b. The data used for analysis were limited to within the transducer response −6 dB bandwidth to minimize possible unreliable or inaccurate data due to processing low-amplitude signals and noise on the attenuation coefficient. The attenuation coefficient variation in a frequency range of 7.5–14.5 MHz for the glaze-like ice sample is shown in Fig. 7.

By comparing the frequency-dependent ultrasonic attenuation in the rime-like and glaze-like ice samples, it can be found that, over the frequency range of 5–15 MHz, while the attenuation increases with frequency in both of the ice samples, at a given frequency, the attenuation has a higher value for the rime-like ice sample. It is also noted that, based on the linear regression lines for the attenuation data, the linear slope ($d\alpha/df$) for the rime-like ice sample is much greater than that for the glaze-like ice sample. It is also seen that there is more scatter in the individual data points for the rime-like ice, which is consistent with scattering in a more complex micromorphology.

IV. Discussion

For the ultrasonic attenuation in other bubble/grain-filled materials, for example, the carbon/epoxy laminates, the attenuation curve typically shows linear behavior with frequency, as seen in Fig. 7, and the curve slope is found to increase as the void content increases [37]. It is therefore suggested that the slope of the attenuation curve for ultrasonic waves in ice is related to the void content in the ice structures.

Table 2 Total densities in ice

Ice type	Total density in ice, g/cm^3	Data source
Rime ice	0.873	Vargas et al. [36]
Rime ice	0.88 ± 0.02	Present study
Glaze ice	$0.857 \sim 0.905$	Vargas et al. [36]
Glaze ice	0.90 ± 0.02	Present study

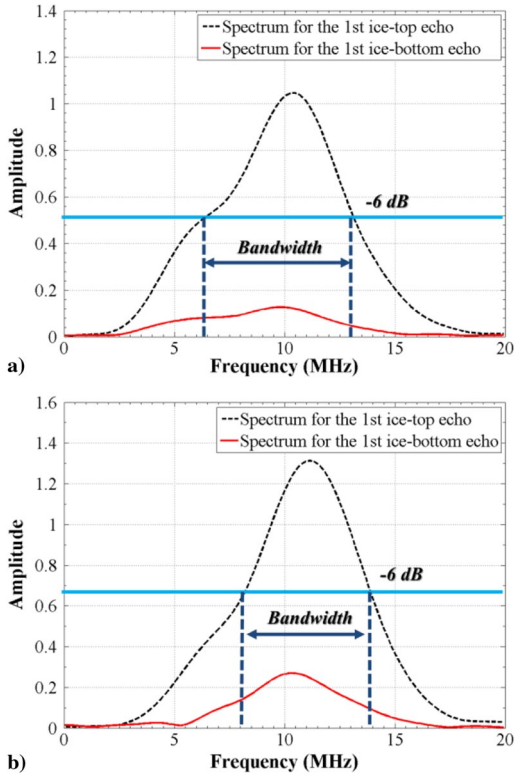

Fig. 6 Amplitude spectra of the ultrasonic echoes for the a) rime-like, and b) glaze-like ice samples.

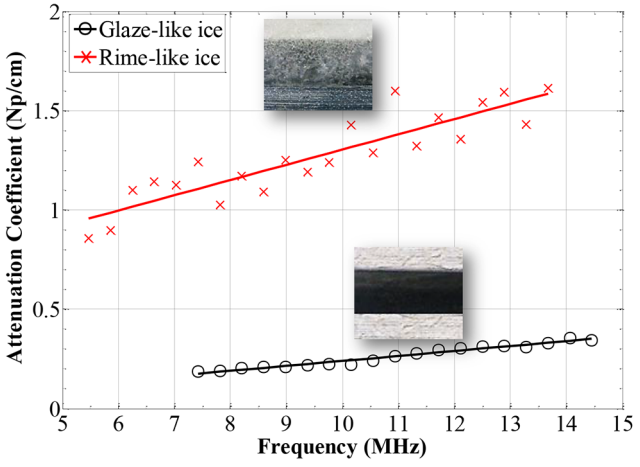

Fig. 7 Frequency-dependent ultrasonic attenuation in the rime-like and glaze-like ice samples.

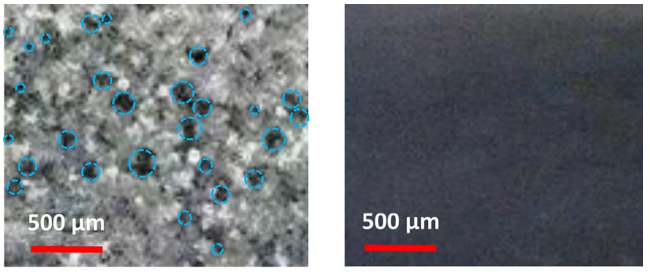

Fig. 8 Microstructures of the rime-like and glaze-like ice samples.

The microstructures of the rime-like and glaze-like ice samples are shown in Fig. 8. It is clear that bubbles of various sizes are randomly distributed in the rime-like ice sample, together with ice grains of various shapes. In contrast, the glaze-like ice is homogeneous, without any observable scattering sources. The void content is estimated to be 9.7% for the rime-like ice sample and 0% for the glaze-like ice sample. It has been previously demonstrated that the acoustic attenuation in ice is typically caused by the wave absorption in ice and the bubble/grain-induced scattering [21].

Table 3 Acoustic attenuation in ice at frequency of 1.1 MHz

Ice type	Acoustic attenuation coefficient, Np/cm	Data source
Sea and freshwater ice	0.173	Bogorodskii et al. [43]
Rime-like Ice	0.374	Present study
Glaze-like Ice	0.102	Present study

In physical acoustics for bubble–ultrasound interaction, there are three distinct scattering regimes, which depend on the magnitude of the parameter $\lambda/2\pi D$, where λ is the wavelength, and D is the diameter of the bubbles/ice grains. In the Rayleigh regime, where $\lambda/2\pi D > 1$, the scattering coefficient is proportional to $D^3 f^4$; in the Stochastic regime, where $0.5 < \lambda/2\pi D < 1$, the scattering increases as a function of Df^2; and in the geometric regime, where $\lambda/2\pi \mathrm{D} < 0.5$, the scattering is no longer dependent on frequency but is inversely proportional to bubble/grain diameter [21].

In the present study, the mean diameter of the air bubbles was estimated to be 100 μm, whereas the ultrasonic wavelength was calculated to be 390 μm. It was calculated that $\lambda/2\pi D_{\text{bubble}}$ is in the 0.5–1 range and therefore that the bubble related scattering is mainly in the stochastic regime, and it is proportional to f^2. The mean diameter of the ice grains in the ice sample was estimated to be 50 μm, and the parameter was calculated to be $\lambda/2\pi D_{\text{grain}} > 1$. The ice-grain caused scattering is therefore in the Rayleigh regime and is proportional to f^4.

The behavior seen in the measured attenuation data in the ice samples suggests that the interaction is the result of the combined effect of different scattering and absorption mechanisms. The equations of the linear regression lines formulated for the attenuation data in the rime-like and glaze-like ice samples are given as Eqs. (17) and (18):

$$\alpha_{\text{rime}}(\text{Np/cm}) = 0.067 \times f(\text{MHz}) + 0.3 \tag{17}$$

$$\alpha_{\text{glaze}}(\text{Np/cm}) = 0.020 \times f(\text{MHz}) + 0.08 \tag{18}$$

The present study considers ultrasonic attenuation in ice at high frequencies (e.g., $f \geq 5.0$ MHz). Although there is a significant literature that considers acoustic and ultrasonic waves in ice (e.g., [37–42]), unfortunately, there is only a limited literature that is available to give data for comparison with that from the present study.

Bogorodskii et al. [43] evaluated the acoustic attenuation in sea and freshwater ice in the frequency range of 200–1100 kHz, and they give attenuation data at $f = 1.1$ MHz. Based on the equations for the linear regression line formulated in this study, the acoustic attenuation at the same frequency (i.e., $f = 1.1$ MHz) can be estimated. The data based on the work by Bogorodskii and the present study were compared, and this is shown in Table 3. It is seen that the attenuation coefficient (nepers per centimeter) reported by Bogorodskii et al. [43] is in between of the data values from the present study for the rime-like and glaze-like ice estimated using the linear equations. The results from the present study are therefore consistent with the limited data that can be deduced from the literature.

V. Conclusions

In the present study, a novel ultrasonic-attenuation-based approach, which is capable of quantitatively characterizing the types (i.e., either rime or glaze) and thickness of the ice accretion pertinent to aircraft icing phenomena, was developed by leveraging the discrepancies in attenuation characteristics of ultrasonic waves traveling in different types of ice. The theories of acoustic attenuation

in pulse-echo configuration for a multilayer structure were formulated with the considerations of interface reflection/transmission, beam diffraction, and the transducer and electronics characteristics. A feasibility study was also carried out to demonstrate the implementation of the ultrasonic-attenuation-based technique by analyzing attenuation characteristics of ultrasonic waves in two different types of ice samples representative of rime and glaze ice accretion typically seen over airframe surfaces.

Significant differences were found in the ultrasonic attenuation characteristics (e.g., the amplitude level, the scattering scale, and the linear slope) between the two compared ice types over the frequency range of 5–15 MHz. The absolute values of the attenuation coefficients for the rime-like ice sample were found to be much greater (i.e., with an excess amplitude varying from 0.75 to 1.2 Np/cm) than those of the glaze-like ice sample at any given frequencies. While the attenuation coefficient was found to increase with the ultrasonic frequency for both ice samples, the increase slope of the attenuation coefficient (i.e., $d\alpha/df$) for the rime-like ice sample was found to be much greater, in comparison to that of the glaze-like ice sample. The measurement data of the ultrasonic attenuation coefficients were also found to have a much wider scattering range for the rime-like ice sample. Such information could be used to develop ice-type-specific anti-/de-icing systems, which could significantly reduce de-icing operational costs and ensure more efficient and safer aircraft operation in cold climate.

Acknowledgment

The research work is partially supported by NASA grant number NNX12AC21A, with Mark Potapczuk as the technical officer, and the Iowa Space Grant Consortium Base Program for Aircraft Icing Studies, with Richard Wlezien as the director. The authors also gratefully acknowledge the support of the National Science Foundation under award numbers CBET-1064196 and CBET-1435590.

References

[1] Smith, W. L., "Weather Problems Peculiar to the New York-Chicago Airway," *Monthly Weather Review*, Vol. 57, No. 12, 1929, pp. 503–506. doi:10.1175/1520-0493(1929)57<503:WPPTTN>2.0.CO;2

[2] Steuernagle, J., Roy, K., and Wright, D., "Aircraft Icing," *AOPA Air Safety Foundation*, Bruce Landsberg, Frederick, MD, 2008.

[3] Bassey, C. E., and Simpson, G. R., "Aircraft Ice Detection Using Time Domain Reflectometry with Coplanar Sensors," *2007 IEEE Aerospace Conference*, Big Sky, MT, 2007, pp. 1–6. doi:10.1109/AERO.2007.352857

[4] Caliskan, F., and Hajiyev, C., "A Review of In-Flight Detection and Identification of Aircraft Icing and Reconfigurable Control," *Progress in Aerospace Sciences*, Vol. 60, July 2013, pp. 12–34. doi:10.1016/j.paerosci.2012.11.001

[5] Gent, R. W., Dart, N. P., and Cansdale, J. T., "Aircraft Icing," *Philosophical Transactions of the Royal Society A: Mathematical, Physical and Engineering Sciences*, Vol. 358, No. 1776, Nov. 2000, pp. 2873–2911. doi:10.1098/rsta.2000.0689

[6] Hansman, R. J., and Kirby, M. S., "Comparison of Wet and Dry Growth in Artificial and Flight Icing Conditions," *Journal of Thermophysics and Heat Transfer*, Vol. 1, No. 3, 1987, pp. 215–221. doi:10.2514/3.30

[7] Thomas, S. K., Cassoni, R. P., and MacArthur, C. D., "Aircraft Anti-Icing and De-Icing Techniques and Modeling," *Journal of Aircraft*, Vol. 33, No. 5, 1996, pp. 841–854. doi:10.2514/3.47027

[8] Gao, H., and Rose, J. L., "Ice Detection and Classification on an Aircraft Wing with Ultrasonic Shear Horizontal Guided Waves," *IEEE Transactions on Ultrasonics, Ferroelectrics, and Frequency Control*, Vol. 56, No. 2, 2009, pp. 334–344. doi:10.1109/TUFFC.2009.1042

[9] Zou, J., Ye, L., and Ge, J., "Ice Type Detection Using an Oblique End-Face Fibre-Optic Technique," *Measurement Science and Technology*, Vol. 24, No. 3, 2013, Paper 35201. doi:10.1088/0957-0233/24/3/035201

[10] Homola, M. C., Nicklasson, P. J., and Sundsbø, P. A., "Ice Sensors for Wind Turbines," *Cold Regions Science and Technology*, Vol. 46, No. 2, 2006, pp. 125–131. doi:10.1016/j.coldregions.2006.06.005

[11] Barre, C., Lapeyronnie, D., and Salaun, G., "Ice Detection Assembly Installed on an Aircraft," U.S. Patent 7000871, Feb. 2006.

[12] Anderson, M., "Electro-Optic Ice Detection Device," U.S. Patent 6425286, July 2002.

[13] Kim, J. J., "Fiber Optic Ice Detector," U.S. Patent 5748091, May 1998.

[14] Abaunza, J. T., "Aircraft Icing Sensors," U.S. Patent 5772153, July 1998.

[15] DeAnna, R., "Ice Detection Sensor," U.S. Patent 5886256, March 1999.

[16] Lee, H., and Seegmiller, B., "Ice Detector and Deicing Fluid Effectiveness Monitoring System," U.S. Patent 5523959, June 1996.

[17] Hansman, R. J., and Kirby, M. S., "Measurement of Ice Growth During Simulated and Natural Icing Conditions Using Ultrasonic Pulse-Echo Techniques," *Journal of Aircraft*, Vol. 23, No. 6, 1986, pp. 492–498. doi:10.2514/3.45334

[18] Hongerholt, D. D., Willms, G., and Rose, J. L., "Summary of Results from an Ultrasonic In-Flight Wing Ice Detection System," *AIP Conference Proceedings*, Vol. 615, No. 1, 2002, pp. 1023–1028. doi:10.1063/1.1472908

[19] Vellekoop, M. J., Jakoby, B., and Bastemeijer, J., "A Love-Wave Ice Detector," *Proceedings of the IEEE Ultrasonics Symposium*, Vol. 1, IEEE Publ., Piscataway, NJ, Oct. 1999, pp. 453–456.

[20] Liu, Q., Wu, K.-T., Kobayashi, M., Jen, C.-K., and Mrad, N., "In-Situ Ice and Structure Thickness Monitoring Using Integrated and Flexible Ultrasonic Transducers," *Smart Materials and Structures*, Vol. 17, No. 4, 2008, Paper 045023. doi:10.1088/0964-1726/17/4/045023

[21] Price, P. B., "Attenuation of Acoustic Waves in Glacial Ice and Salt Domes," *Journal of Geophysical Research*, Vol. 111, No. B2, 2006, pp. 2156–2202. doi:10.1029/2005JB003903

[22] Abbasi, R., et al., "Measurement of Acoustic Attenuation in South Pole Ice," *Astroparticle Physics*, Vol. 34, No. 6, 2011, pp. 382–393. doi:10.1016/j.astropartphys.2010.10.003

[23] Gudra, T., and Najwer, L., "Ultrasonic Investigation of Snow and Ice Parameters," *Acta Physica Polonica, A*, Vol. 120, No. 4, 2011, pp. 625–629. doi:10.12693/APhysPolA.120.625

[24] Liu, Y., Chen, W., Bond, L. J., and Hu, H., "A Feasibility Study to Identify Ice Types by Measuring Attenuation of Ultrasonic Waves for Aircraft Icing Detection," *4th Joint US-European Fluids Engineering Division Summer Meeting Collocated with the 12th International Conference on Nanochannels, Microchannels, and Minichannels*, American Soc. of Mechanical Engineers Paper FEDSM2014–21227, Chicago, Aug. 2014.

[25] Svilainis, L., "Review of High Resolution Time of Flight Estimation Techniques for Ultrasonic Signals," *2013 International Conference NDT*, Telford, England, U.K., Sept. 2013, pp. 1–12.

[26] Schmerr, L. W., "Material Attenuation and Efficiency Factors," *Fundamentals of Ultrasonic Nondestructive Evaluation*, Plenum, New York, 1998, pp. 283–304.

[27] Ensminger, D., and Bond, L. J., *Ultrasonics: Fundamentals, Technologies, and Applications*, CRC Press, Boca Raton, FL, 2011, pp. 27–139.

[28] Rogers, P. H., and Van Buren, A. L., "An Exact Expression for the Lommel-Diffraction Correction Integral," *Journal of the Acoustical Society of America*, Vol. 55, No. 4, 1974, pp. 724–728. doi:10.1121/1.1914589

[29] Krautkrämer, J., and Krautkrämer, H., *Ultrasonic Testing*, 4th ed., Springer–Verlag, New York, 1990, p. 41.

[30] Potapczuk, M. G., "Aircraft Icing Research at NASA Glenn Research Center," *Journal of Aerospace Engineering*, Vol. 26, No. 2, 2013, pp. 260–276. doi:10.1061/(ASCE)AS.1943-5525.0000322

[31] Hansman, R. J., and Kirby, M. S., "Measurement of Ice Accretion Using Ultrasonic Pulse-Echo Techniques," *Journal of Aircraft*, Vol. 22, No. 6, 1985, pp. 530–535. doi:10.2514/3.45160

[32] Liu, Y., Bond, L. J., and Hu, H., "Reconstruction of Wave Features in Wind-Driven Water Film Flow Using Ultrasonic Pulse-Echo Technique," *AIP Conference Proceedings*, Vol. 1706, 2016, Paper 020015. doi:10.1063/1.4940461

[33] Vogt, C., Laihem, K., and Wiebusch, C., "Speed of Sound in Bubble-Free Ice," *Journal of the Acoustical Society of America*, Vol. 124, No. 6, 2008, pp. 3613–3618. doi:10.1121/1.2996304

[34] Abbasi, R., et al., "Measurement of Sound Speed vs. Depth in South Pole Ice for Neutrino Astronomy," *Astroparticle Physics*, Vol. 33, Nos. 5–6, 2010, pp. 277–286.

[35] Filipczynski, L., Pawlowski, Z., and Wehr, J., *Ultrasonic Methods of Testing Materials*, Butterworths, London, 1966.

[36] Vargas, M., Broughton, H., Sims, J. J., Bleeze, B., and Gaines, V., "Local and Total Density Measurements in Ice Shapes," *Journal of Aircraft*, Vol. 44, No. 3, 2007, pp. 780–789. doi:10.2514/1.23326

[37] Jeong, H., and Hsu, D. K., "Experimental Analysis of Porosity-Induced Ultrasonic Attenuation and Velocity Change in Carbon Composites," *Ultrasonics*, Vol. 33, No. 3, 1995, pp. 195–203. doi:10.1016/0041-624X(95)00023-V

[38] Umchid, S., "Frequency Dependent Ultrasonic Attenuation Coefficient Measurement," *3rd International Symposium on Biomedical Engineering (ISBME)*, 2008, pp. 234–238.

[39] Wu, P., and Stepinski, T., "Quantitative Estimation of Ultrasonic Attenuation in a Solid in the Immersion Case with Correction of Diffraction Effects," *Ultrasonics*, Vol. 38, No. 1, 2000, pp. 481–485. doi:10.1016/S0041-624X(99)00037-2

[40] Treiber, M., Kim, J.-Y., Jacobs, L. J., and Qu, J., "Correction for Partial Reflection in Ultrasonic Attenuation Measurements Using Contact Transducers," *Journal of the Acoustical Society of America*, Vol. 125, No. 5, 2009, pp. 2946–2953. doi:10.1121/1.3106125

[41] Zeng, F., Agnew, S. R., Raeisinia, B., and Myneni, G. R., "Ultrasonic Attenuation Due to Grain Boundary Scattering in Pure Niobium," *Journal of Nondestructive Evaluation*, Vol. 29, No. 2, 2010, pp. 93–103. doi:10.1007/s10921-010-0068-2

[42] Selfridge, A. R., "Approximate Material Properties in Isotropic Materials," *IEEE Transactions on Sonics and Ultrasonics*, Vol. 32, No. 3, 1985, pp. 381–394. doi:10.1109/T-SU.1985.31608

[43] Bogorodskii, V. V., Gavrilo, V. P., and Nikitin, V. A., "Sound Propagation in Ice Crystallized from Salt-Water," *Soviet Physics Acoustics*, Vol. 22, No. 2, 1976, pp. 158–159.

C. Wen
Associate Editor